

# Sensing liquid density using resonant flexural plate wave devices with sol-gel PZT thin films

Jyh-Cheng Yu · Huang-Yao Lin

The original publication is available at [www.springerlink.com](http://www.springerlink.com), <http://dx.doi.org/10.1007/s00542-007-0550-7>

Received: 30 June 2007 / Accepted: 28 December 2007  
Springer-Verlag 2008/2/12

**Abstract** This study presents the design, fabrication and possible applications in liquid density sensing and biosensing of a flexure plate wave (FPW) resonator using sol-gel-derived lead zirconate titanate (PZT) thin films. The resonator has a two-port structure with a reflecting grating on a composite membrane of PZT and SiN<sub>x</sub>. The design of the reflecting grating is derived from a SAW resonator model using COM theory to generate a sharp resonant peak. A comparison between the theoretical mass and the viscosity effects reveals the applications and the constraints of the proposed device in liquid sensing. Multiple coatings of sol-gel-derived PZT films are employed because of the cost advantage and the strong electromechanical coupling effect over other piezoelectric films. Issues of fabrication of the proposed material structure are addressed. Theoretical estimates of the mass and the viscosity effects are compared with the experimental values. The resonant frequency relates quite linearly to the density of low-viscosity liquids, revealing the feasibility of the proposed device.

## 1. Introduction

Acoustic wave devices have attracted substantial attention for sensor applications owing to the sensitivity of wave velocity and damping to external disturbances such as

temperature, pressure, additive mass and viscosity [1]. The phase velocity of Lamb waves, unlike the velocity of surface acoustic wave (SAW), depends on the thickness of the plate in which they propagate. They can be treated as two strongly coupled Rayleigh waves that propagate on both sides of the plate. Two vibrating modes can propagate through the plate independently, as symmetric and the anti-symmetric Lamb modes. The anti-symmetric zero mode, A<sub>0</sub>, also called the “flexural plate wave” (FPW), which propagates on a thin plate with a thickness of 5% or less of the acoustic wavelength, can be designed to have a phase velocity that is lower than the velocity of sound in the loading liquid. A slow mode of propagation will reduce the radiation energy loss and make FPW devices effective in liquid sensing.

Lamb waves are most readily excited and detected using interdigital transducers (IDTs) [2] on a thin piezoelectric plate that is fabricated by the etching of a bulk substrate. Reflecting gratings are added to the FPW devices, as was first reported by Joshi [3], using a Y-X lithium niobate plate to increase the differentiability and the sensitivity of the resonant frequency shift. Nakagawa[4] employed the same configuration but on an AT-cut quartz substrate.

Piezoelectric thin films are less expensive than crystalline materials, explaining the considerable interest owing to the possible applications. Laurent *et al.* [5] addressed the configuration design of the FPW devices using AlN and ZnO on silicon membrane, indicating that the FPW device has a greater mass sensitivity than other acoustic devices. Costello *et al.*[6] developed a simple theory for the mass sensitivity of a delay-line oscillator with ZnO on a silicon nitride membrane, and modeled the attenuation of plate waves in contact with viscous liquids. Weinberg *et al.*[7] derived the fluid-damping model of resonant FPW devices.

---

J.-C. YU\* AND H.-Y. LIN  
Department of Mechanical and Automation Engineering,  
National Kaohsiung First University of Science and Technology,  
2, Juoyue Rd., Nantz District, Kaohsiung 811, TAIWAN, ROC.  
\* Corresponding Author: [jcyu@ccms.nkfust.edu.tw](mailto:jcyu@ccms.nkfust.edu.tw)

J.-C. Yu  
Center for Micro/Nano Science and Technology,  
National Cheng Kung University  
No.1, Ta-Hsueh Road, Tainan 701, TAIWAN, ROC.

The electromechanical coupling effect and the dielectric constant of PZT markedly exceed those of AlN and ZnO, making PZT films attractive for sensor applications. Also, sol-gel deposition [8] is promising because its need for a deposition facility is much less expensive than sputtering and chemical vapor deposition (CVD). Typical sol-gel processes include the preparation of precursor, spin coating and heat treatment. However, the polycrystalline structure of PZT and the high temperature of the annealing process may cause the cracking and diffusion of structure layers. The deposition of buffer layers, such as LSMO, between the PZT thin film and the structure layers can improve the piezoelectric characteristics, fatigue resistance and ferroelectricity, and reduce leaking current [9]. Also, the use of excess Pb in the preparation of precursor can compensate for the volatilization of Pb during annealing [10].

Although many studies have addressed possible applications of FPW devices, the mass, tensile stress and viscosity effects may become coupled when the device is in contact with the liquid, affecting sensing selectivity. Very few works have addressed the practical issues that are raised in sensor fabrication and measurement and are important in liquid and biological sensing. This investigation will consider the design and the fabrication of an FPW resonator using sol-gel-derived PZT on silicon nitride membrane. Mass loading when the device is in contact with the liquid will introduce a deviation in the resonant frequency that is determined by the liquid density and viscosity. The limitations on the proposed device in liquid density sensing are presented. The investigation of fabrication issues will cover the effect of material structure and process parameters on the realization of the device. Finally, the experimental results are compared with the theoretical estimates.

## 2. Design of FPW Resonator

The proposed FPW resonator utilizes a two-port IDT and two reflectors on a composite membrane that comprises piezoelectric layers, a buffer layer and a silicon nitride-supporting membrane. Figure 1 schematically depicts the device. The thickness of the composite membrane is suggested to be 5% or less of the acoustic wavelength  $\lambda$  to excite the lowest mode of the flexural plate wave. For fluid and biosensing applications, the phase velocity of the acoustic wave must be smaller than the velocity of sound in water to reduce the radiation energy loss. Other design parameters are determined by the tradeoff between the device size and sensitivity. More pairs of IDT correspond to smaller insertion loss and larger bandwidth. Increasing the overlap length of IDT reduces the insertion loss and

increases the transmission effect. The proposed device assumes 20 pairs of electrodes in both IDTs, the overlap length of IDT to be  $50\lambda$ , and the separation between the IDTs to be  $10\lambda$ .

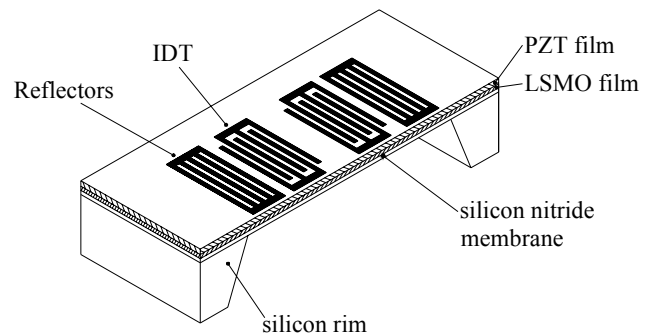


Figure 1 Schematic View of FPW resonators

The design of the reflecting grating is based on a two-port SAW resonator over a bulk PZT that is modeled using COM theory [13]. The modeling of a typical SAW resonator has three basic elements - IDT, spacing and reflector which can be described by three complex transmission matrices [T], [D] and [G], respectively, as presented in Figure 2. Matrix [T] is a  $3 \times 3$  transmission matrix for the IDTs, including both acoustic and electric parameters. The terms,  $a$  and  $b$ , represent the incident and the reflected electrical signals, respectively. Matrix [D] is a  $2 \times 2$  matrix for the acoustic transmission line between IDTs and gratings. Matrix [G] is a  $2 \times 2$  matrix for the SAW reflection grating that specifies the relationship between the acoustic transmission and reflection responses  $W_i$ .

If the output IDT has no input electrical signal, then the overall acoustic modeling can be simplified as follows;

$$[W_0] = [M][W_7] + a_3[G_1][D_2][\tau_3] \quad (1)$$

where  $[M] = [G_1][D_2][T_3][D_4][T_5][D_6][G_7]$  and  $\tau_3$  is the column matrix that relates to the input coupling.

Assume absorbers are applied to the outside of both reflection gratings; no acoustic wave is incident on grating  $G_1$  or  $G_7$ .

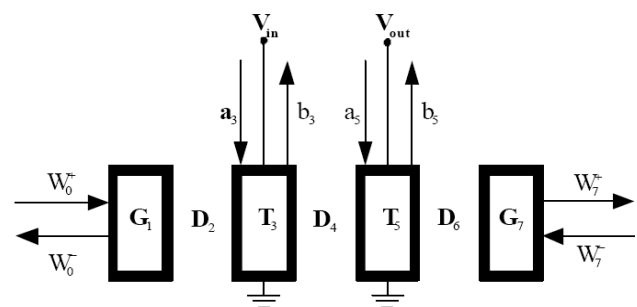


Figure 2 Representation of two-port resonator building blocks

$$W_0^+ = W_7^- = 0 \tag{2}$$

Substituting the boundary conditions to Eq. (1) yields

$$\begin{bmatrix} 0 \\ W_0^- \end{bmatrix} = [M] \begin{bmatrix} W_7^+ \\ 0 \end{bmatrix} + a_3 [G_1] [D_2] [\tau_3] \tag{3}$$

From the transmission matrices in Fig. 2,  $b_5$  is given by

$$b_5 = [\tau_5'] \cdot [W_5] \tag{4}$$

where  $\tau_5'$  is a column vector that relates to the output coupling. The output IDT generally has no incident electrical signal. The transmission coefficient  $S_{21}$  can then be estimated as follows;

$$S_{21}|_{a_5=0} = b_5 / a_3 \tag{5}$$

The simulation parameters herein are as follows; acoustic wavelength is 40  $\mu\text{m}$  with uniform finger spacing, and the phase velocity of bulk PZT is 2400 m/s. The reflection phase,  $\theta$ , is determined by the position of the standing wave at the reference plane, which relates to the sign of the reflected-to-incident surface waves that enter the reflection grating, influencing the designed spacing between the gratings and the adjacent IDTs ( $D_2$  and  $D_6$ ). Determining the reflecting phase is difficult and commonly depends on the experimental results for the combination of the piezoelectric substrate and the reflecting electrodes [13]. The reflection coefficient for the combination of the PZT thin film and the Pt/Ti reflecting grate is unavailable. However, since PZT is a strong piezoelectric, like lithium niobate, the reference phase  $\theta = 0^\circ$  is assumed in the open circuit design of a reflector. The number of the reflection grating is set to 40 to generate standing waves and thus reduce insertion loss. As presented in Fig. 3, the spacing between the gratings and the adjacent IDTs will influence

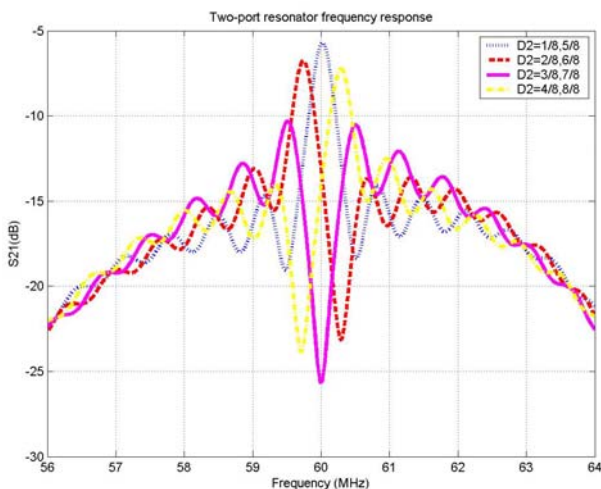


Figure 3 Two-port SAW resonator frequency response

the resonant pattern, and ( $D_2$ ) is designed to be  $(1/8+n/2)\lambda$  to produce a sharp resonant peak. The derived reflector design is applied to the FPW device to increase the differentiability of the frequency deviation associated with liquid loading.

### 3. Sensing Mechanism of FPW Device

#### 3.1. Estimation of phase velocity

Consider the  $A_0$  mode of an FPW that propagates on a thin plate; the phase velocity of the plate regime is given by a simple asymptotic expression [12]:

$$v_p = \left( \frac{B}{M} \right)^{1/2} \tag{6}$$

where  $B = \left( \frac{\lambda}{2\pi} \right)^2 \frac{E'd^3}{12}$  is the bending stiffness of a homogeneous plate,  $E' = E/(1-\nu^2)$  is the effective Young's modulus,  $E$  is the actual Young's modulus,  $\nu$  is Poisson's ratio,  $d$  is the plate thickness, and  $M$  is the mass per unit area of a homogeneous isotropic plate.

The material structure of the proposed FPW device is assumed to be Pt (0.15 $\mu\text{m}$ ) / Ti (0.02 $\mu\text{m}$ ) / PZT (1 $\mu\text{m}$ ) / LSMO (0.1 $\mu\text{m}$ ) / SiN<sub>x</sub> (1.2 $\mu\text{m}$ ). Table 1 presents the mechanical properties of the material system [14]. The PZT properties are assumed from those of the bulk material. The (La<sub>x</sub>Sr<sub>1-x</sub>)MnO<sub>3</sub>, LSMO, is a buffer layer between PZT and SiN<sub>x</sub>. The material properties of LSMO are unavailable and assumed to be the same as that of the PZT film. The mass effect of the Pt and the Ti are negligible.

The total thickness of the composite membrane is 2.3  $\mu\text{m}$ . The material parameters of the composite membrane, as presented in Table 1, are estimated using composite plate theory. The phase velocity estimated using Eq. (7) is 235.1 m/s, and the resonant frequency of the device in air is  $f_{\text{air}} = 5.88$  MHz at a wavelength of 40  $\mu\text{m}$ .

Table 1 Material properties of the composite plate

	SiN <sub>x</sub>	PZT / LSMO
Thickness ( $\mu\text{m}$ )	1.2	1 (PZT) + 0.1 (LSMO)
Young's modulus ( $E$ , N/m <sup>2</sup> )	$3.85 \times 10^{11}$	$8.6 \times 10^{10}$
Poisson ratio ( $\nu$ )	0.27	0.25
Density ( $\rho$ , kg/m <sup>3</sup> )	3100	7600
$M$ (kg/m <sup>2</sup> )	0.00372	0.00836

#### 3.2. Loading effects of contact liquid

When the device is in contact with liquid, an additional stiffness effect is introduced by the weight of the liquid and

the additional mass associated with the agitation of the liquid. The phase velocity of the plate regime under tensile stress and liquid loading can be well approximated, as follows [12].

**Table 2** Parameters of the composite membrane

$E$	$2.42 \times 10^{11}$ (N/m <sup>2</sup> )
$M$	0.1176 (N/m <sup>2</sup> )
$\nu$	0.26
$E'$	$2.6 \times 10^{11}$ (N/m <sup>2</sup> )
$B$	6497.93 (N/m)

$$v_p = \left( \frac{T_x + B}{M + \rho_F \delta_E + M_\eta} \right)^{1/2} \quad (7)$$

where  $T_x$  is the component of in-plane tension in the  $x$  direction,  $\rho_F \delta_E$  is the mass effect,  $\delta_E$  is the evanescent decay length,  $\rho_F$  is the density of the fluid, and  $M_\eta$  is the viscosity effect.

Equation (8) gives the evanescent decay length, and can be further simplified if the phase velocity is much less than the velocity of sound in the contact liquid.

$$\delta_E = \left( \frac{\lambda}{2\pi} \right) \left[ \left( 1 - \frac{v_p}{v_F} \right)^2 \right]^{-1/2} \approx \left( \frac{\lambda}{2\pi} \right) \quad (8)$$

The viscosity effect is the product of the liquid density and the viscous decay length:

$$M_\eta = \frac{\rho_F \delta_V}{2} \quad (9)$$

where  $\delta_V = \left( \frac{2\eta}{\omega \rho_F} \right)^{1/2}$  is the viscous decay length,  $\omega$  is the operating angular frequency, and  $\eta$  is the shear viscosity.

### 3.2.1. Loading of low-viscosity liquids

In Eq.(7), the viscosity effect for a low-viscosity liquid is negligible and the phase velocity is influenced solely by the mass effect ( $\rho_F \delta_E$ ) that is determined by the evanescent decay length. However, if the loading liquid is a small droplet on the thin plate and the contacting surface is not hydrophilic, then the droplet does not spread out uniformly but remains hemispherical, as displayed in Fig. 4. Since only the evanescent decay length of the loading droplet contributes to the mass loading effect and the shape of the droplet cannot be accurately controlled, the change in the phase velocity is normally not proportional to the number of liquid droplets. Hence, the liquid is suggested to fill up the cavity if the device is used to detect the mass effect. The liquid density determines the low-viscosity liquid loading as long as the filled liquid level exceeds the evanescent decay length, as shown in Fig. 5.

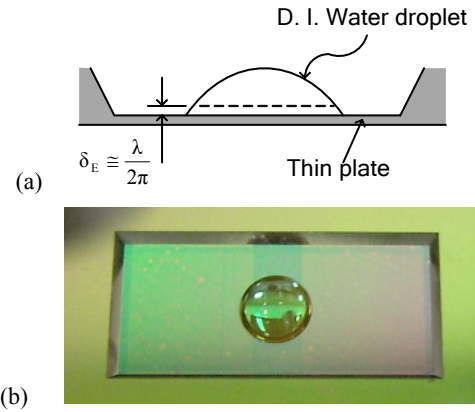


**Figure 4** Liquid droplet on the FPW device (a) Schematic cross section (b) Photo using digital camera

The weight of the liquid introduces tensile stress to the membrane, resulting in the deviation of the phase velocity. The sensitivities of the perturbation of the phase velocity to mass and tension are as follows.

$$\frac{\Delta v_p}{v_p} = s_m \times \rho_F + s_T \times T_x \quad (10)$$

where  $s_m = -\frac{\delta_E}{2(M + \rho_F \delta_E)}$  and  $s_T = \frac{1}{2(T_x + B)}$

The calculated phase velocity of the composite membrane in air is approximately  $235 \text{ m}\cdot\text{s}^{-1}$  which is much less than the speed of sound in water, which is  $1482 \text{ m}\cdot\text{s}^{-1}$ . The stiffness of the membrane is estimated using composite plate theory. The calculated sensitivities in the case considered herein are  $s_m = -2.78 \text{ m}^2/\text{N}$  and  $s_T = 7.69 \times 10^{-5} \text{ m/N}$ . If 5 mg of water is loaded on the cavity, the mean tensile stress in the wave propagating direction can be estimated by performing a finite element analysis. The estimated frequency deviation due to the mass loading of water is around -0.94 MHz and the frequency deviation due to the tensile effect is only +1.24 KHz. The tension effect due to the liquid pressure is negligible by comparison with the mass loading effect.

When the device cavity is filled with different liquids, the resonant frequency deviation relates to the liquid density, and so can be used as a density sensor. The phase velocity of the FPW device loaded with three low-viscosity liquids can be estimated, as presented in Table 3.

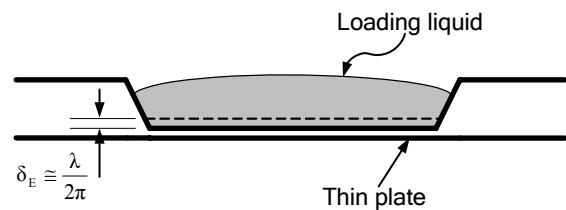


**Figure 5** Evanescent decay length for the liquid loading in a FPW device

**Table 3** Estimated resonant frequency of the FPW device loaded with low-viscosity liquids

	IPA	Water	Saline solution
Viscosity Ns/m <sup>2</sup>	0.0025	0.001	~0.0015
Phase Velocity (m/s)	197.48	190.05	183.77
Resonant Frequency (MHz)	4.94	4.75	4.59

### 3.2.2. Loading of viscous liquids

Equation (7) demonstrates that the fluid density ( $\rho_F$ ) and shear viscosity ( $\eta$ ) of the loading liquid affect the phase velocity of FPW. However, the contributions of liquid density and viscosity to the velocity perturbations cannot be distinguished because the density and the viscosity are coupled in the viscosity effect, as revealed by Eq. (9). Restated, the liquid viscosity cannot be determined by the frequency shift. Hence, the proposed device is unsuitable for measuring the density and viscosity of viscous liquids only from the resonant frequency deviation.

## 4. Device Fabrication

### 4.1. Fabrication Procedure

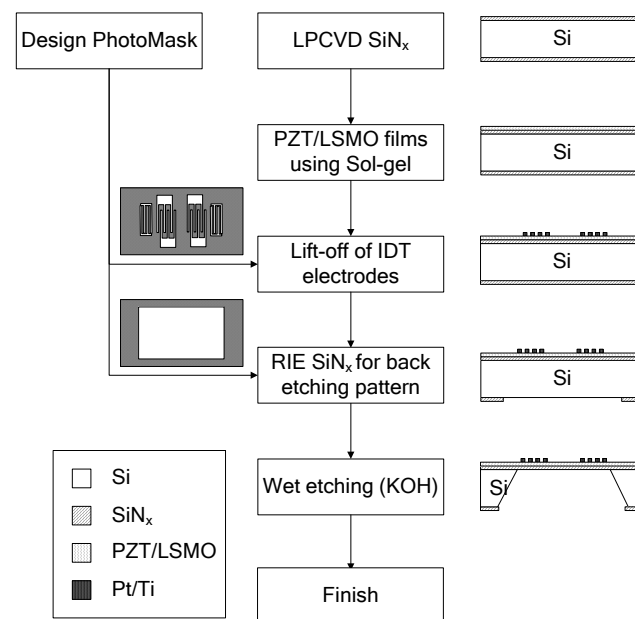
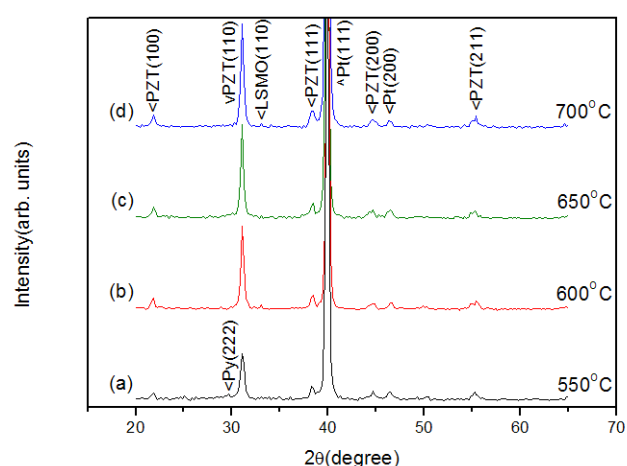
Figure 6 presents the procedure for fabricating the FPW resonator with a piezoelectric layer coating, silicon etching and the lift-off of IDT. The material system of the resonator is assumed Pt/Ti/PZT/LSMO/SiN<sub>x</sub>. The LSMO and the PZT thin films were multiple-coated using sol-gel procedures. The electrodes of the IDT were deposited using E-beam PVD and patterned with period of 40  $\mu\text{m}$  using lift-off. The back cavity was then patterned on SiN<sub>x</sub> using RIE. Finally, the membrane cavity of the device was fabricated using KOH anisotropic etching (30°C, 80%). The final composite membrane comprised 1.2  $\mu\text{m}$  silicon nitride and 1.1  $\mu\text{m}$  PZT layers, and the size of the membrane was approximately 4.2  $\times$  2.7mm.

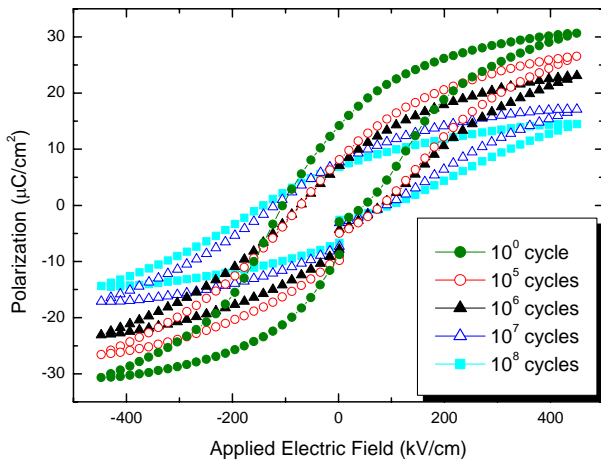
### 4.2. Sol-Gel Deposition of PZT

The sol-gel PZT thin films require heat treatment to be transformed into polycrystalline piezoelectric layers. Furnace heating is performed herein this study. Increasing the heat treatment temperature may improve the material characteristics of PZT, but severe thermal stresses may crack the film because of incompatibility among constituent layers of the composite membrane. Figure 7 presents the X-ray diffraction pattern of four layers of PZT that was annealed at various temperatures for 30 min. The experimental results show that the heat treatment of PZT

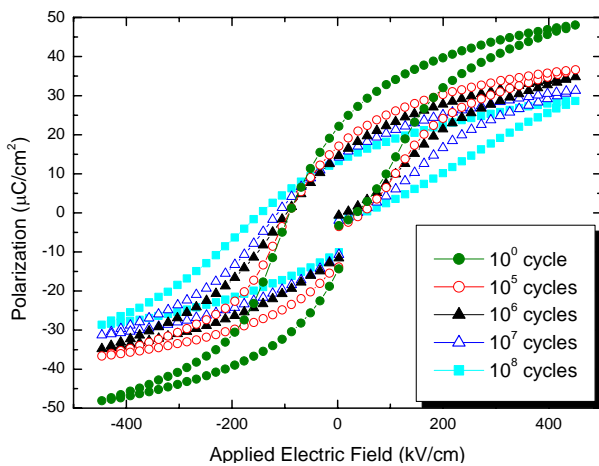
films at 650°C yields satisfactory perovskite structures without a pyrochlore phase.

The LSMO coating is used as a buffer layer between PZT and SiN<sub>x</sub>; it enhances the piezoelectric characteristics and prevents possible cracking of PZT. A comparison of Figs. 8 and 9 demonstrates that the LSMO buffer layer not only enhances residual polarization but also reduces the polarization decay by fatigue loading that is very important for resonant devices.


**Figure 6** Fabrication procedure of the FPW resonator

**Figure 7** XRD of PZT (4L)/LSMO/Pt/Ti/SiO<sub>2</sub>/Si at various annealing temperatures for 30 min.



**Figure 8** Fatigue characteristics for the PZT film without LSMO buffer layer



**Figure 9** Fatigue characteristics for the PZT film with LSMO buffer layer

## 5. Experimental Results and Discussion

### 5.1. FPW delay line and FPW resonator signals

The frequency responses of the FPW delay line and the FPW resonator are measured using a network analyzer (HP8753 ES). Figure 10 plots the frequency responses of the FPW delay line and the FPW resonator. The measured resonant frequency without liquid loading is 5.53 MHz, which is quite close to the theoretical estimate of 5.88 MHz. The difference may follow from the use of the bulk material properties in the theoretical estimate since the PZT film properties are unknown. The resonator has a more obvious resonant signal than the delay line design, although no sharp peak is observed, perhaps because PZT has a polycrystalline structure.

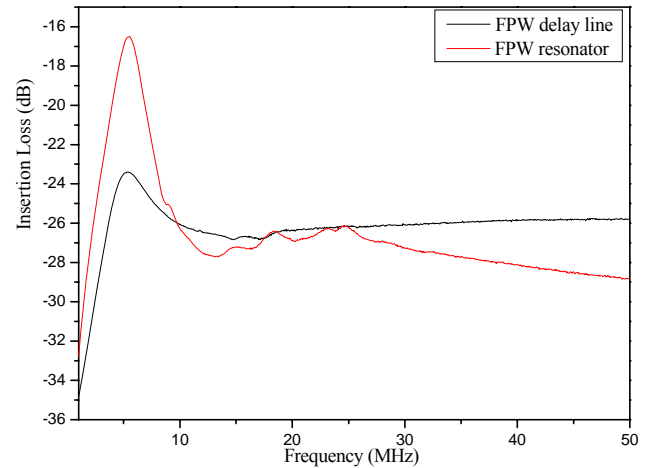


**Figure 10**  $S_{21}$  frequency response of the FPW devices

### 5.2. Liquid sensing using FPW resonator

Three low-viscosity liquids, DI Water ( $1 \text{ g/cm}^3$ ), IPA ( $0.787 \text{ g/cm}^3$ ) and saline solution ( $1.2 \text{ g/cm}^3$ ), are applied to the resonator. The viscosity effect is negligible compared with the mass effect. Figure 11 analyzes the sensitivity of the resonant frequency and the densities of the liquids. The theoretical relative density sensitivity for low-viscosity liquids is  $-0.848 \text{ (MHz/g}\cdot\text{cm}^3)$ . The results show that the resonant frequency and the liquid density are strongly linearly correlated (despite a static difference between the theoretical and experimental curves, which demonstrates the feasibility of density sensing. The static difference may be due to the use of bulk material properties in the theoretical estimates and liquid damping which was presumed to be negligible.

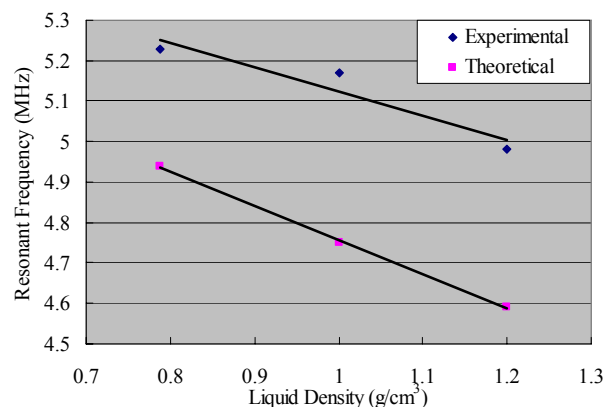


**Figure 11** Sensitivity analysis of the resonant frequency and the density of low-viscosity liquids

However, theoretical analysis indicates that fluid density and shear viscosity of a high-viscosity liquid affect the phase velocity of FPW. The contributions of liquid density and viscosity to velocity perturbations cannot be

distinguished because they are coupled in the viscosity effect. Restated, the liquid viscosity cannot be determined from the frequency shift. Herein, two liquids, glycerol with a viscosity of  $934 \times 10^{-3}$  (Ns/m<sup>2</sup>) is compared with a low-viscosity saline solution of the same density (1.2 g/cm<sup>3</sup>) to investigate the viscosity effect.

Table 4 shows that glycerol loading introduces an additional frequency deviation above that of the saline solution of the same density. Also, the viscosity effect of glycerol causes greater dampening than does that of the saline solution and increases the insertion loss.

**Table 4** Viscosity effect on the resonant frequency and insertion loss

	Theoretical Frequency (MHz)	Experimental	
		Frequency (MHz)	Insertion Loss (dB)
Saline solution	4.59	4.98	-33.38
Glycerol	4.49	4.73	-37.04

## 6. Conclusions

This work fabricated the FPW resonator on PZT piezoelectric thin films and compared the measurement results with the modeling analysis. The fabrication process is presented and the effect of the process parameter is investigated. Adding the LSMO buffer layer improves the surface interface and the sensor reliability. Although the polycrystalline structure of PZT may obscure the resonant peak of the frequency response, the peak is sufficient to differentiate the frequency deviation due to liquid loading. The device is loaded with various liquids. Liquid loading increases the insertion loss and reduces the resonant frequency in a manner consistent with theoretical prediction. The linear correlation between the resonant frequency and the density of a low-viscosity liquid shows the feasibility of density sensing. Additional frequency deviation and insertion loss are observed when high-viscosity liquids are applied to the device, which results are consistent with the theoretical estimation. However, the proposed device cannot differentiate the velocity perturbations associated with liquid density and viscosity, which prevent the application of the device to the measurement of the density of high-viscosity liquid by frequency deviation alone. The accompanying increase in the insertion loss due to liquid viscosity may be considered to identify the liquid.

**Acknowledgements** The authors would like to thank the National Science Council of the Republic of China, Taiwan, for financially supporting this research under Contract No. NSC 93-2216-E-327-001.

## References

- [1]. Vellekoop, M. J., Acoustic wave sensors and their technology, *Ultrasonic*, Vol.36, pp. 7-14, 1998
- [2]. White, R. M. and Voltmer, F. M. "Direct piezoelectric coupling to surface elastic waves", *Appl. Phys. Lett.*, Vlo. 7, pp. 314-316, 1965.
- [3]. Joshi, S. G. and Zaitsev, B. D., Reflection of ultrasonic Lamb waves propagating in thin piezoelectric plates, *Ultrasonics Symposium*, pp.423-426, 1998
- [4]. Nakagawa, Y., Momose, M. and Kakio, S., Characteristics of reflection of resonators using Lamb wave on AT-cut quartz, *Japanese Journal of Applied Physics*, Vol. 43, pp. 3020-3023, 2004
- [5]. Laurent, T., Bastien, F. O., Pommier, J.-C., Cachard, A., Remiens, D., and Cattan, E., Lamb wave and plate mode in ZnO/silicon and AlN/silicon membrane Application to sensors able to operate in contact with liquid, *Sensors and Actuators*, pp. 26-37, 2000
- [6]. Costello, B. J., Martin, B. A., and White, R. M. Ultrasonic plate waves for biochemical measurements, *Ultrasonics Symposium*, pp. 977-981, 1989
- [7]. Weinberg, M. S., Dubé, C. E., Petrovich, A., and Zapata, A. M., Fluid damping in resonant flexural plate wave device, *Journal of Microelectromechanical Systems*, Vol. 12, No. 5, pp. 567-576, 2003.
- [8]. Pan, H.-C., Tsai, H.-L. and Chou, C.-C., "Low-Temperature Preparation of PbZrTiO<sub>3</sub>/Pt/TiN/Si Heterostructure by Laser Annealing", *Integrated Ferroelectrics*, v. 46, pp. 163-173, 2002.
- [9]. Chen, M. S., Wu, T. B., Wu, J. M., "Effect of Textured LaNiO<sub>3</sub> Electrode on the Fatigue Improvement of Pb(Zr<sub>0.53</sub>Ti<sub>0.47</sub>)O<sub>3</sub> Thin Films", *Appl. Phys. Lett.*, 68[10], pp. 1430-1432, 1996.
- [10]. Wang, Z. J., Maeda, R. and Kikuchi, K., "Effect of Pb Content on Electric Properties of Sol-Gel Derived Lead Zirconate Titanate Thin Films Prepared by Tree-Step Heat Treatment Process", *Jpn. J. Appl. Phys.*, Vol. 38, pp. 5342-5345, 1999
- [11]. Matsui, Y., Okuyama, M., Fujita, N., and Hamakawa, Y., "Laser annealing to produce ferroelectric-phase PbTiO<sub>3</sub> thin films", *J. Appl. Phys.* 52(8), pp. 5107-5111, 1981.
- [12]. White, R. M. et al., *Acoustic Wave Sensors Theory, Design, and Physico-Chemical Applications*, Academic Press, 1996.
- [13]. Campbell, C. K., *Surface acoustic wave devices for mobile and wireless Communications*, San Diego: Academic Press, 1998.
- [14]. [http://www.piezo-kinetics.com/PKI\\_700.htm](http://www.piezo-kinetics.com/PKI_700.htm)